SIMULATION OF ORBITAL FORMING PROCESS USING 3D FEM AND INVERSE ANALYSIS FOR DETERMINATION OF RELIABLE FLOW STRESS

H. Cho[(1)], N. Kim[(2)], and T. Altan[(1)]

[(1)] ERC for Net Shape Manufacturing, The Ohio State University
339 Bakers Systems Building, 1971 Neil Avenue, Columbus OH, 43210 USA

[(2)] Dept. of Mechanical Engineering, Sogang University
Shinsoo-dong, Mapo-gu 1, Seoul, 121-742 Korea

Summary

In this study the feasibility of 3D FEM simulation of the orbital forming process was investigated by evaluating the simulation time. Commercial FEA software DEFORM™ 3D v4.0 that has an efficient computation algorithm for simulating incremental forming process was used for the simulations and the savings in computation time was determined. In order to provide reliable flow stress for the simulation, a finite element based inverse analysis technique has been introduced. Results show that developed inverse analysis technique is efficient and accurate for use in 3D FEM simulation for process optimization.

1. Introduction

The finite element simulation technique is a popular and powerful tool to improve the forging sequences and the quality of forgings at industry. The applications of 2D FEM to practical industrial problems began in the late 1980s. By using FEM simulation, the influence of individual design parameters involved in forming operations on forged part could be investigated easily. Recently, thanks to increase in computing speed, efforts on combining FEM simulation with optimization algorithm are being made in order to optimize the manufacturing operations [1,2]. Also, the use of 3D FEM simulation keeps growing rapidly. However, in spite of improvement of computing speed, the associated cost of 3D FEM simulation is still expensive. Further reducing computation time is still a key to make 3D FEM simulation practical, efficient, and robust for industrial applications.

In using user-friendly commercial FEA software it is necessary to assign reliable input data since the results of process simulation are extremely sensitive to the accuracy of flow stress and interface friction that are input to FEM programs. It is essential that these input values are determined using appropriate material tests and the evaluation of the test results should be able to overcome difficulties frequently introduced by inhomogeneous deformation. Even in the simple cylinder compression, interface friction leads to an inevitable bulging of the sample and affects flow stress determination. Thus, it is better to consider the unavoidable friction at the tool/workpiece interface in the test and to identify it together with flow stress using the inverse analysis. In the inverse analysis, the unknown parameters are determined by minimizing a least-square functional consisting of experimental data and FEM simulated data. The FEM is used to analyze the behavior of the material during the test, whereas the optimization technique allows for automatic adjustment of parameters until the calculated response matches the measured one within a specified tolerance [3].

In this study, based on rigid-plastic finite element formulation, a new inverse analysis algorithm has been developed. This analysis identifies the material strength constant and strain hardening exponent of the flow stress equation by minimizing a least-square functional consisting of experimental load and predictions

made by FEM simulation. Furthermore, a methodology for simultaneous determination of flow stress and interface friction has been introduced. Also, in order to investigate a feasibility of application to 3D FEM simulation, as an example, 3D FEM simulations of orbital forming process were performed.

2. Reliable flow stress determination

2.1 Inverse analysis algorithm

The basic concept of an inverse analysis for parameter identification is to compute a set of unknown material parameters $\boldsymbol{p}$, which represents the flow stress curve. The unknown parameters are determined by minimizing an objective function, $E(\boldsymbol{p})$, representing the difference between the experimental and corresponding computed loads in a least-square sense:

$$E(\boldsymbol{p}) = \frac{1}{N}\sum_{i=1}^{N}\left(\frac{F_i - f_i(\boldsymbol{p})}{F_i}\right)^2 \tag{1}$$

where F is the experimentally measured load and f is the computed load. N is the number of data sampling points in a load vs. stroke curve used to construct the objective function. For a given set of material parameters, the objective function will be minimum at:

$$\frac{\partial E(\boldsymbol{p})}{\partial p_k} = 0 \quad \text{for } k = 1,\ldots,m \tag{2}$$

where m is the number of parameters to be identified.

The equation (2) is solved with respect to the parameters p_k using Newton-Raphson iterative method.

$$\frac{\partial^2 E}{\partial p_k \partial p_j}\Delta p_j = -\frac{\partial E}{\partial p_k} \quad \text{for } k, j = 1,\ldots,m \tag{3}$$

The first and second derivatives of the objective function with respect to the parameters p_k are evaluated by taking the derivatives of Equation (1) with respect to material parameters p_k:

$$\frac{\partial E}{\partial p_k} = -\frac{2}{N}\sum_{i=1}^{N}\left\{\frac{(F_i - f_i)}{F_i}\frac{\partial f_i}{\partial p_k}\right\} \tag{4}$$

$$\frac{\partial^2 E}{\partial p_k \partial p_j} = -\frac{2}{N}\sum_{i=1}^{N}\left\{-\frac{\partial F_i}{\partial p_k}\frac{\partial f_i}{\partial p_j} + (F_i - f_i)\frac{\partial^2 f_i}{\partial p_k \partial p_j}\right\} \tag{5}$$

where the computed force f_i is defined in rigid-plastic FEM as follows [4]:

$$f_i = \sum_{\mathrm{e}}\int_{\mathrm{V^e}} \frac{2}{3}\frac{\bar{\sigma}}{\dot{\bar{\varepsilon}}}\boldsymbol{B}^T\boldsymbol{D}\boldsymbol{B}\mathrm{dV}\hat{\boldsymbol{v}} + \sum_{\mathrm{e}}\int_{\mathrm{V^e}} \mathrm{G}\boldsymbol{B}^T\boldsymbol{c}\boldsymbol{c}^{\mathrm{T}}\boldsymbol{B}\mathrm{dV} \tag{6}$$

$\bar{\sigma}$ is the effective stress, which is equal to the flow stress of material during the plastic deformation, $\dot{\bar{\varepsilon}}$ is the effective strain rate, $\boldsymbol{B}$ is the strain rate-nodal velocity matrix, and G is the penalty constant respectively. $\boldsymbol{D}$ and $\boldsymbol{c}$ are a matrix and a vector of constant components. Thus, f_i, $\frac{\partial f_i}{\partial p_k}$, and $\frac{\partial^2 f_i}{\partial p_k \partial p_j}$ are calculated using Equations (6)-(8) only for tool-contacting elements.

$$\frac{\partial f_i}{\partial p_k} = \sum_{\mathrm{e}}\int_{\mathrm{V^e}} \frac{2}{3}\frac{1}{\dot{\bar{\varepsilon}}}\left(\frac{\partial \bar{\sigma}}{\partial p_k}\right)\boldsymbol{B}^T\boldsymbol{D}\boldsymbol{B}\mathrm{dV}\hat{\boldsymbol{v}} \tag{7}$$

$$\frac{\partial^2 f_i}{\partial p_k \partial p_j} = \sum_{\mathrm{e}}\int_{\mathrm{V^e}} \frac{2}{3}\frac{1}{\dot{\bar{\varepsilon}}}\left(\frac{\partial^2 \bar{\sigma}}{\partial p_k \partial p_j}\right)\boldsymbol{B}^T\boldsymbol{D}\boldsymbol{B}\mathrm{dV}\hat{\boldsymbol{v}} \tag{8}$$

For a strain hardening material, the flow stress equation may be given by $\bar{\sigma} = K\bar{\varepsilon}^n$. The first and second derivatives of the flow stress equation with respect to material strength constant K and strain hardening exponent n are expressed by Equation (9).

$$\frac{\partial \bar{\sigma}}{\partial p_k} = \begin{Bmatrix} \frac{1}{K}\bar{\sigma} \\ (\ln\varepsilon)\bar{\sigma} \end{Bmatrix}, \quad \frac{\partial^2 \bar{\sigma}}{\partial p_k \partial p_j} = \begin{bmatrix} 0 & \frac{\ln\varepsilon}{K}\bar{\sigma} \\ \frac{\ln\varepsilon}{K}\bar{\sigma} & (\ln\varepsilon)^2\bar{\sigma} \end{bmatrix} \tag{9}$$

The optimal amount of adjustments for material parameters Δp_k is found after solving Equation (3). Then material parameters are improved iteratively until Equation (2) is satisfied using the following equation.

$$p_k^{(\mathrm{i}+1)} = p_k^{(\mathrm{i})} + \Delta p_k \tag{10}$$

At the next optimization step a new FEM simulation is conducted with improved material parameters and this procedure is repeated until the deviation of material parameters becomes within tolerance. The flow chart of this algorithm is shown in Figure 1.

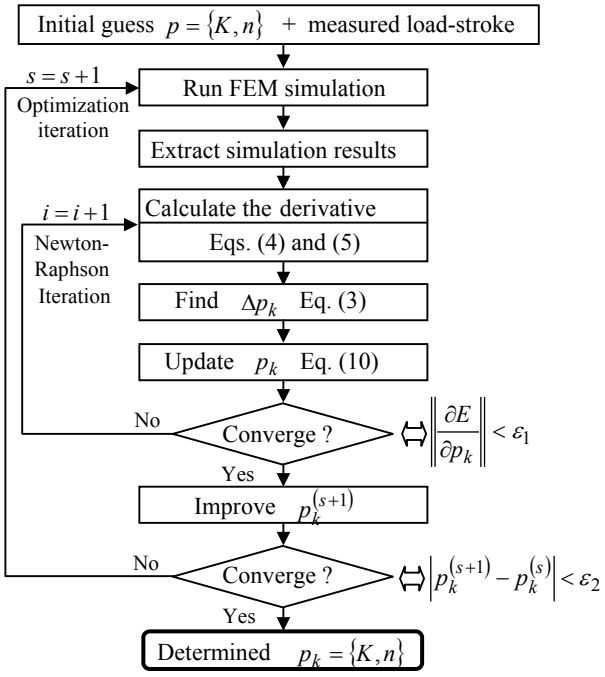

Figure 1: Flow chart of inverse analysis.

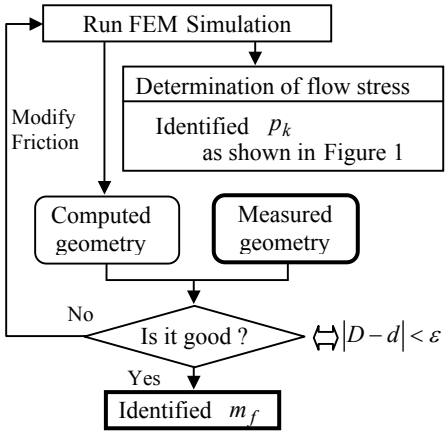

Figure 2: Flow chart for determination of flow stress and friction factor by the inverse analysis.

2.2 Inverse analysis of non-homogeneous cylinder compression.

The developed inverse analysis algorithm has been tested by using the real experimental data obtained from the cylinder compression test of AISI 1022. Cylinder with 0.4 inch height x 0.265 inch diameter was compressed at the reduction of 45%. During the compression, a barreling was observed due to the existing frictional force at the die/specimen interface. In order to determine reliable flow stress, the effect of existing frictional force has to be taken into account in the inverse analysis. For this purpose, two experimental quantities: (1) the load-stroke curve and (2) the barreling shape (bulge diameter) of the cylinder specimen at the end of stroke were measured and flow stress and interface friction are determined simultaneously. As explained as the flow chart in Figure 2, flow stress is first determined by minimizing the difference in the load-stroke curves. Then, the unknown friction factor is identified by comparing the measured bulge diameter and its corresponding computed diameter.

Table 1: Predicted inverse analysis results.

Friction m_f	Bulge diameter [in], (Error %)	K-value (Mpa)	n-value
0.1	0.363 (- 0.7)	113.5	0.138
0.15	0.366 (- 0.11)	113.1	0.138
0.2	0.368 (+ 0.56)	112.9	0.139

The results of identified parameters (K-value and n-value) in the flow stress equation and friction factor by the inverse analysis are summarized in Table 1. Three inverse analyses were conducted by varying the friction factor from 0.1 to 0.2. As initial guesses of material parameters $K=130$ and $n=0.2$ were used for every case. When the friction factor 0.15 was assumed, the inverse analysis prediction produced only 0.11% underestimation in bulge diameter comparison. Thus, a combination of friction factor $m_f=0.15$ and flow stress $\bar{\sigma}=113\bar{\varepsilon}^{0.138}(Mpa)$ gives the best matches both in load-stroke curve and bulge diameter comparisons. As shown in Figure 3, after four optimization iterations, the computed and experimental loads are nearly identical.

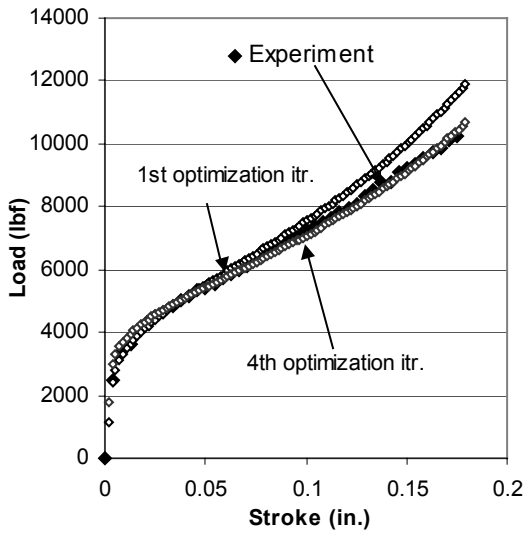

Figure 3: Comparison of computed and experimental load stroke curves.

In Figure 4, the measured bulge diameter from the test and the computed bulge diameter from the simulation were compared at the same stroke position. When friction factor was 0.15, they showed a good match.

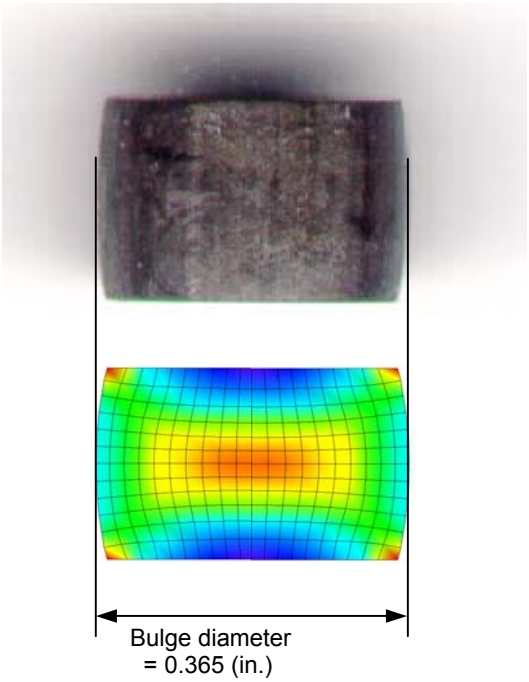

Figure 4: Comparison of measured (top) and computed (bottom) bulge diameters at the end of stroke with $\bar{\sigma} = 113\bar{\varepsilon}^{0.138}(Mpa)$ and $m_f = 0.15$.

The convergence behaviours of the material parameters $P_k = \{K, n\}$ during optimization iteration were shown in Figure 5 and Figure 6, respectively. In both cases, monotonously converging behaviors were observed.

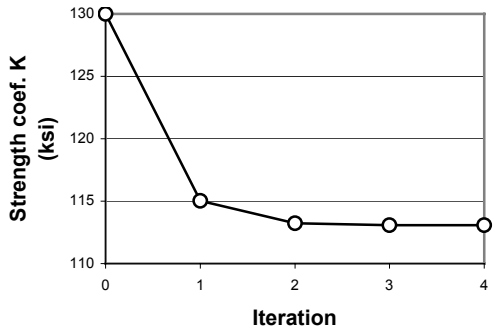

Figure 5: Convergence of material strength coefficient, K.

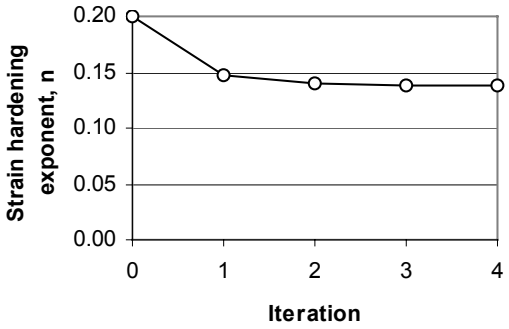

Figure 6: Convergence of strain hardening exponent, n.

3. Simulation of orbital forming

3.1 Orbital forming of wheel spindle bearing

Orbital forming is an incremental forming process in which the conventional overall compression of the billet is replaced by localized incremental deformation of the billet until the final shape is formed. The tool is tilted at small angle with respect to the axis of the lower die and the tool rotates and moves axially as it completes its stroke. When orbital forming is used for assembly of automotive wheel spindle bearings, the orbiting tool deforms the forged spindle material gradually so as to create an axial clamping force, Figure 7. This axial force acts through the inner ring and keeps the bearing pre-loaded and retained.

Since the orbital forming is an incremental forming process, it requires a number of revolutions to form a part. For FEM simulation, a relatively large number of simulation steps are required to minimize the errors in solution accuracy. Also, a full 3D modeling is required due to an asymmetric rotational tool movement.

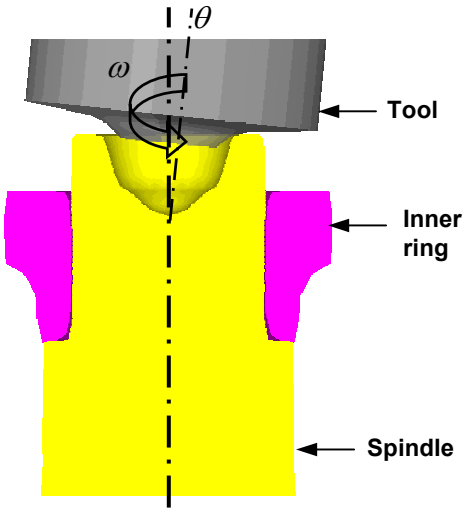

Figure 7: Principle of orbital forming of wheel spindle bearing.

3.2 Simulation conditions

The FE model of spindle was generated with 9875 nodes and 43231 tetrahedral elements. The finer mesh system was created near the tab region to have an accurate prediction of metal flow. The spindle material is assumed to show rigid-plastic deformation behavior and flow stress of $\bar{\sigma} = 113\bar{\varepsilon}^{0.138}(Mpa)$ determined by inverse analysis was used in the simulation. The tool and the inner ring were regarded as rigid objects and shear friction factor of 0.15 was used in the simulations, assuming lubricated conditions. From a given movement of the orbital tool, 500 simulation steps are assigned and time step size was determined as 0.0025 (sec/step). In the simulation, this time step size provides 48 incremental steps for simulating one revolution of the orbit tool. Figure 8 shows generated finite element models for the 3D simulation. In order to evaluate how efficient the new computation method of DEFORM^{TM} 3D v4.0 for simulating orbital forming process, one simulation was conducted using the new efficient solution method and the other simulation was carried out by inactivating the new solution method. As a default, new solution method is automatically activated in DEFORM^{TM} 3D v4.0.

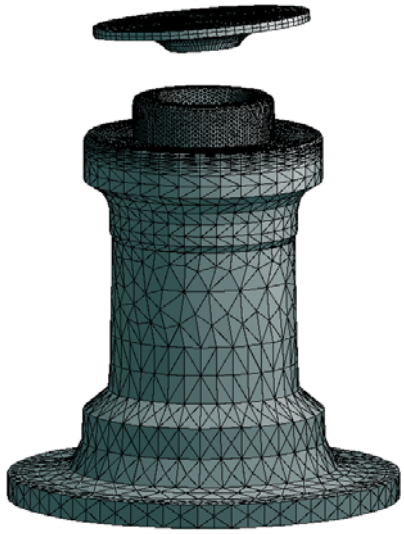

Figure 8: 3D Finite element model for orbital forming simulation.

3.3 Simulation results

In Table 1, the results of two simulations are summarized. When the simulation was made in DEFORM^{TM} 3D v4.0, 8 hrs. 12 min. CPU time was required to complete the stroke. However, when the new solution method was inactivated the CPU time was dramatically increased up to 98 hrs. Therefore, around 91% saving of computation time was achieved. The difference between the predicted maximum forming forces is about 2.5 % and between the predicted tab outer diameters is about 0.5 %, respectively. This comparison indicates that the simulation results made with the enhanced solution method are nearly identical to the results obtained with conventional solution method.

Table 2: Comparison of consumed CPU time.

	Activating new method	Inactivating new method
Overall CPU time	8 hrs. 12 min.	98 hrs.
CPU Time / Itr.	0.5~1.0 sec.	30~40 sec.

(Machine: HP J6000 w/2GB Memory)

In Figure 9, the predicted metal flow at different punch strokes near the tab of the spindle are shown. The predicted outer tab diameter is defined in Figure 9 (c).

(a) After 40% punch stroke

(a) After 80% punch stroke

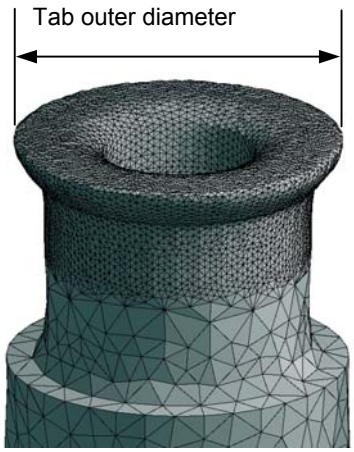

(c) At the end of punch stroke

Figure 9: Predicted metal flow of spindle at intermediate stages.

4. Conclusions and discussion

In this study, simulation of orbital forming for assembly of wheel spindle bearing was conducted using commercial FE software DEFORM^{TM} 3D v4.0, which recently introduced an efficient computation numerical algorithm for simulating incremental forming processes. It is concluded that the computation time required for simulating an incremental forming process has been significantly reduced by 91 % in spite of the nature of incremental forming process where a large number of simulation steps are needed with a full 3D finite element modeling. Solution accuracy was verified by comparing the predicted forces and tab outer diameters and they showed good agreements. Therefore, the use of 3D FEM in simulating and optimizing the orbital forming seems to be a reasonably reliable tool for process and tool design in this process.

Also, in order to provide reliable flow stress for the simulation, finite element based inverse analysis technique was developed to identify the material strength constant and strain hardening exponent of the flow stress equation. The results indicated that with this method it was possible to predict the flow stress and friction simultaneously with acceptable accuracy.

References

[1] L. Fourment and J. L. Chenot, Optimal Design For Non-Steady-State Metal Forming Processes-I. Shape Optimization Method, Int. J. Numerical Methods in Eng., Vol. 39, pp. 33-50, 1996.

[2] G. Zhao, E. Wright, and R. V. Grandhi, Sensitivity Analysis Based Preform Die Shape Design For Net-Shape Forging, Int. J. Mach. Tools Manufact., Vol. 37, No. 9, pp. 1251-1271, 1997.

[3] J. L. Chenot, E. Massoni, and L. Fourment, Inverse Problems in Finite Element Simulation of Metal Forming Processes", Engineering Computations, Vol. 13, No. 2/3/4, p. 190-225, 1996.

[4] S. Kobayashi, S.-I. Oh, and T. Altan, Metal Forming and Finite Element Method, Oxford University Press, NY, 1989